Linear Viscoelasticity from Molecular Dynamics Simulation of Entangled Polymers

Alexei E. Likhtman,*,† Sathish K. Sukumaran, and Jorge Ramirez†

Department of Applied Mathematics, University of Leeds, Leeds LS2 9JT, U.K.

Received April 10, 2007; Revised Manuscript Received July 3, 2007

ABSTRACT: The linear viscoelastic (LVE) spectrum is one of the primary fingerprints of polymer solutions and melts, carrying information about most relaxation processes in the system. Many single chain theories and models start with predicting the LVE spectrum to validate their assumptions. However, until now, no reliable linear stress relaxation data were available from simulations of multichain systems. In this work, we propose a new efficient way to calculate a wide variety of correlation functions and mean-square displacements during simulations without significant additional CPU cost. Using this method, we calculate stress−stress autocorrelation functions for a simple bead−spring model of polymer melt for a wide range of chain lengths, densities, temperatures, and chain stiffnesses. The obtained stress−stress autocorrelation functions were compared with the single chain slip−spring model in order to obtain entanglement related parameters, such as the plateau modulus or the molecular weight between entanglements. Then, the dependence of the plateau modulus on the packing length is discussed. We have also identified three different contributions to the stress relaxation: bond length relaxation, colloidal and polymeric. Their dependence on the density and the temperature is demonstrated for short unentangled systems without inertia.

1. Introduction

The main challenge of entangled polymer dynamics is replacing the many chains system by a single chain moving in an effective self-consistent field. In the first approximation, this field is assumed to be tubelike, ensuring that at some length scales the chain moves only parallel to itself.[1] Although the tube theory can successfully explain many experimental results,[2] it lacks a microscopic foundation and fails to answer many questions on the length scale of the order of the tube diameter. Such questions include the following.

- What is the entanglement or tube field restricting the chain motion?
- Why does it not contribute to the stress? (or does it?)
- What are the statistical properties of the tube? For instance, is it semiflexible on the length scale of tube diameter?
- What is the microscopic basis for the assumptions used to describe constraint release in the linear and the nonlinear regimes?
- What happens to the entanglements and the tubes after large deformations or in fast flows?
- How does the branch point diffuse inside the tube?

Beyond these, many numerical parameters in the tube theories are unknown and are usually assumed to be unity. Examples include the ratio of the tube diameter to the tube Kuhn length, the ratio of the friction inside the 1-d tube to that in unentangled systems, the analogous ratio of the spring constants etc. The more detailed slip−spring model[3] can answer some of these questions, but many of its assumptions still lack microscopic foundations, most notably the constraint release mechanism and the relation between virtual spring strength and the number of these springs.

The most promising way to build the microscopic foundation for the tube or the slip-links models is using molecular dynamics simulations of many entangled chains. Molecular dynamics of entangled polymers was pioneered by Kremer and Grest.[4] They showed almost 20 years ago that it was already possible to simulate a minimal polymer model exhibiting some signs of entanglements. At about the same time, Gao and Weiner[5] dedicated several papers to the analysis of the microscopic stresses in molecular dynamics simulations. Since these seminal papers, many molecular dynamics algorithms have significantly improved. In particular, several new methods were proposed for the initial system preparation.[6,7] However, the stress relaxation of entangled polymers in the linear regime (the most basic rheological function), has remained inaccessible. In their papers, Gao and Weiner mainly reported the stress relaxation after a large extension ($\lambda = 2$). Recently, Sen. et al.[8] calculated the stress−stress autocorrelation function of the standard Kremer−Grest model and claimed to have observed a plateau for the chain length $N = 120$. Zhou and Larson[9] rightly attributed this to noise in Sen's simulations (see Figure 3, and the corresponding discussion). Recently, Zhou and Larson[9] have calculated the stress relaxation function for one particular semiflexible system, but did not investigate it in detail. In this paper we use a new efficient method of calculating correlation functions over many decades in time (up to 8 decades in our case) without significant additional CPU cost. Using this method has allowed the calculation of the stress relaxation functions for a wide variety of systems both with and without bending energy and for different densities and temperatures. Although this paper answers none of the questions posed earlier, it provides a starting point for a more detailed comparison with the single chain models, which will follow in a subsequent publication.[10]

In the next section, we will describe the model used in the simulations and the method for calculating correlation functions. Then we will present and discuss in detail the stress relaxation function and the mean square monomer displacements for the standard Kremer−Grest model. We will also briefly discuss the cross-correlations between different chains. Then, we will

* Corresponding author. E-mail: A.Likhtman@reading.ac.uk.
† Present address: Department of Mathematics, University of Reading, Whiteknights, PO Box 220, Berkshire, RG6 6AX, U.K.

10.1021/ma070843b CCC: $37.00
Published on Web 08/14/2007

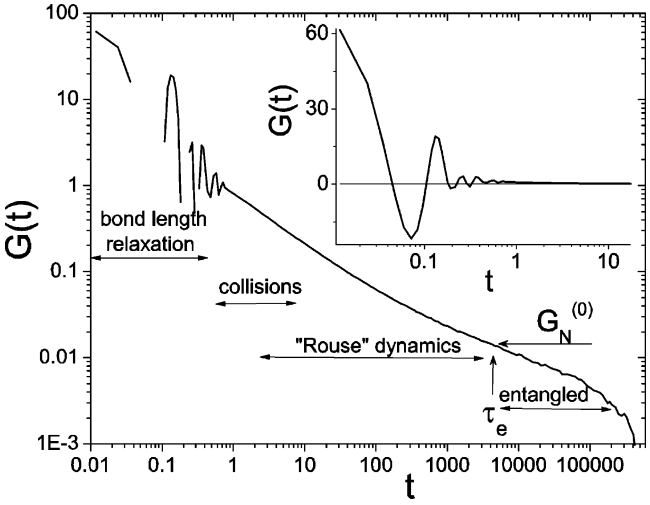

Figure 1. Stress relaxation for the standard KG model, $N = 350$. The inset shows the same data at an early time in log−linear scale.

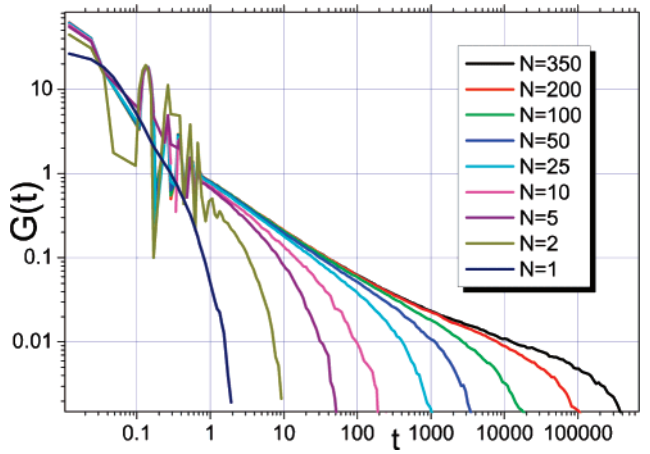

Figure 2. Stress relaxation for the standard KG model.

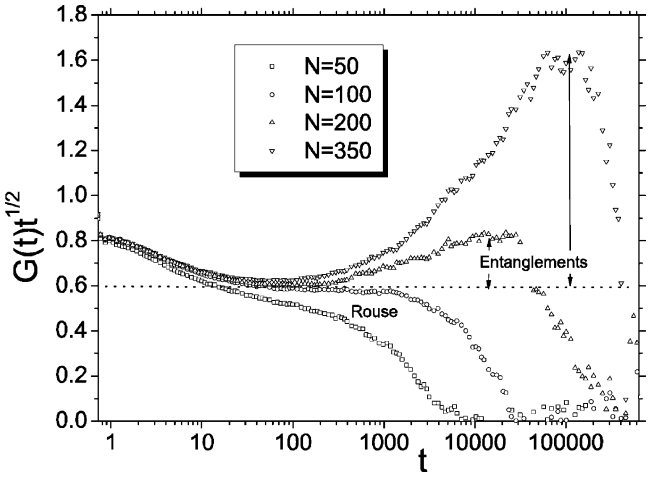

Figure 3. Stress relaxation for the four longest chains $N = 50$, 100, 200, and 350 of the standard model, normalized by the Rouse behavior $t^{-1/2}$. A horizontal line on this plot corresponds to pure Rouse behavior.

explore the change in the stress relaxation function with density and temperature and identify three different contributions to the stress. In the next section, we will discuss the stress relaxation for chains with bending energy and the dependence of the plateau modulus on the packing length. The last section will list the conclusions of the paper.

2. Model and Correlators

The model we use needs no introduction: it is exactly the same model used by Kremer and Grest(KG).[4] It consists of purely repulsive Lennard-Jones beads connected by FENE springs, and the strength of the springs is adjusted so that the chains cannot cross each other:

$$U_{LJ}(r) = 4\epsilon((\sigma/r)^{12} - (\sigma/r)^6 + 1/4),\ r/\sigma < 2^{1/6};$$
$$U_{FENE}(r) = -kR_0^2/2\ \ln(1 - (r/R_0)^2)$$

where $R_0 = 1.5\sigma$ is the spring's maximum extension and $k = 30\epsilon/\sigma^2$ is the spring constant. All quantities below will be expressed in the units where the Lennard-Jones energy ϵ, Lennard-Jones radius σ and the particle's mass m are equal to unity. In particular, the elementary bond length relaxation time scale is $\tau_0 = \sigma\sqrt{m/\epsilon}$, and the unit of stress is ϵ/σ^3. Temperature ($k_BT = \epsilon$) is maintained using a Langevin thermostat with friction $\zeta = 0.5$, and the monomer density is $\rho = 0.85$ unless specified otherwise. We will refer to this parameter set as the standard model.

It is worthwhile to ponder the reasons why reliable stress relaxation functions for entangled systems were not calculated in the 17 years after the Kremer−Grest and the Gao−Weiner papers. The typical stress−stress autocorrelation function is shown in Figure 1 for a chain length $N = 350$ standard KG model in log−log scale and on log−linear scale for early times in the inset. Looking at the log−linear plot one may be tempted to conclude that all the stresses have relaxed at $t \approx 1$ since the amplitude of initial oscillations is significantly larger than the amplitude of all other processes. The log−log plot is much more revealing: it shows a total span of relaxation times of almost 8 decades, and this is just for a mildly entangled polymer (the number of entanglements Z is about 7; see later).

The plot illustrates two major difficulties in measuring the stress relaxation due to entanglements in molecular dynamics: (1) The time step has to be about 3×10^5 times smaller than the characteristic time τ_e, where entangled dynamics starts to appear. Since multichain simulations typically do not exceed 10^8 steps, we have only 2.5 decades of "interesting" information to collect. (2) The value of the plateau modulus ($\approx 10^{-2}$) is almost 4 decades lower than the amplitude of stress fluctuations $G(0)$ due to bond length relaxation and other modes. Thus, the signal-to-noise ratio must be much higher than 10^4 in order to obtain accurate information about the plateau modulus and the shape of the stress relaxation at long times.

It is obvious from Figure 1 that for accurate results the stress has to be calculated at every time step. Indeed, if we calculate the stress autocorrelation function using, say, every tenth point, the noise at long times is much larger due to inaccurate averaging over the bond fluctuations. However, storing 10^8 values of several components of stress is rather expensive (files of 20 Gb or so), and postprocessing of these files is time-consuming. The way around these problems is a correlator algorithm widely used in photon-correlation spectroscopy.[11,12] The algorithm involves an array of correlators, each correlator containing P numbers ($P = 16$ in our case). The first correlator contains the instantaneous stress values; the second one contains the averages of M neighboring values etc. (we use $M = 2$). At every time step, the stress is calculated and placed in the first cell of the first correlator, pushing all other values in this correlator to the right. The numbers arriving to each correlator are also added to an accumulator; when M values are added, the accumulator is divided by M and sent to the next correlator,

and the accumulator is set to zero again. The early time correlation function (first P points) is calculated using the first correlator, then the next $P(1 - 1/M)$ values are calculated using second correlator, etc. Thus, for long times, instead of calculating correlations of instantaneous values of the stress, we calculate correlations of average stress, and the averaging time is about P times smaller than the argument of the correlation function. In other words, the use of correlator involves the following approximation

$$F(\tau) \equiv \frac{1}{T-\tau}\int_0^{T-\tau} f(t+\tau)f(t)\,dt \simeq \frac{1}{T-\tau}\left(\frac{P}{\tau}\right)^2 \times \int_0^{T-\tau-\tau/P} dt \int_{-\tau/P}^{0} f(t+\tau+t')\,dt' \times \int_{-\tau/P}^{0} f(t+t'')\,dt'' = \left(\frac{P}{\tau}\right)^2 \int_0^{\tau/P} dt' \int_0^{\tau/P} dt''\, F(\tau+t'-t'') \quad (1)$$

The error in this approximation is controlled by P and M and is shown to be below 1% for $P = 16$, $M = 2$ for decaying correlation functions.[11] The last expression in eq 1 shows that this approximation is similar to running averages used in refs,[8,9] but we have the significant advantage of calculating all averages on the fly without having to store and postprocess large volumes of data. More detailed descriptions of the correlator and error analysis will be published separately.[12]

Using this correlator algorithm, we can routinely calculate a large variety of correlation functions for the entire time range without a serious loss of CPU resources. We have also created a correlator for the calculation of the mean-square displacement of particle i, $g_1(i, t)$. In this case, one needs a separate correlator for each particle in the simulation box and a small correction for each correlator since g_1 is not a decaying function (see ref 12 for more details). In order to improve the signal-to-noise ratio further, each simulation presented in this paper was averaged over 8−10 independent runs. Each run was performed on a single 2.2 Ghz AMD processor, and the longest run ($N =$ 350 standard setting) took almost a year. The performance of the code developed in house is about 1.5 μs per time step per particle for large systems.

As reported in the literature,[7] system preparation is one of the most challenging steps. Since the preparation methods developed in the literature are empirical, we used some of them (i.e., good initial guess for single chain statistics plus slow push off), but always allowed chains to reptate several times before starting calculations of the relaxation modulus and other quantities. Because of high precision achieved due to use of correlators, we found that we can easily detect poorly prepared systems. In particular, they showed high apparent plateau in $G(t)$ and the $g_1(i, t)/t^{1/2}$ for middle monomers showed no overlap at early times for different molecular weights. Mean square internal distances $\langle(R_i - R_j)^2\rangle/|i - j|$ were closely monitored for all systems as described in ref 7 and overlapped well between different chain lengths for the same bending energy and density.

3. Results

3.1. Stress Relaxation. We start our discussion by presenting the stress relaxation functions for the standard model for different chain lengths. Figure 2 shows $G(t)$ for N ranging from 1 to 350, with the longest relaxation function spanning 7.5 decades in time. The $N = 1$ case corresponds to a Lennard-Jones liquid and does not show any oscillations. The curve for $N = 2$ shows the largest oscillations, and all other curves collapse onto a master curve at early times. Although there is no clear entanglement plateau even for the longest chain $N =$ 350 (corresponding roughly to seven entanglements—see later), one can clearly see the inflection point and upward deviation from the Rouse relaxation (slope higher than −1/2). In order to amplify the deviations from the Rouse theory, we plot $t^{1/2}G(t)$ for $N = 50-350$ (Figure 3). This plot has two advantages—the y axis becomes very compressed (i.e., all changes can be shown in less than one decade), and all the deviations from the Rouse theory are easily seen as deviations from the horizontal line. In particular, we observe that for $t < 30$ there are deviations from the Rouse model with the slope about −0.63. This will be discussed in section 4. In contrast to ref,[8] who claimed to see a plateau in the stress−stress autocorrelation function for $N =$ 120, we see that for a similar length $N = 100$ the slope of $G(t)$ does not deviate from the Rouse behavior, although the viscosity and terminal time do (see Table 1 later).

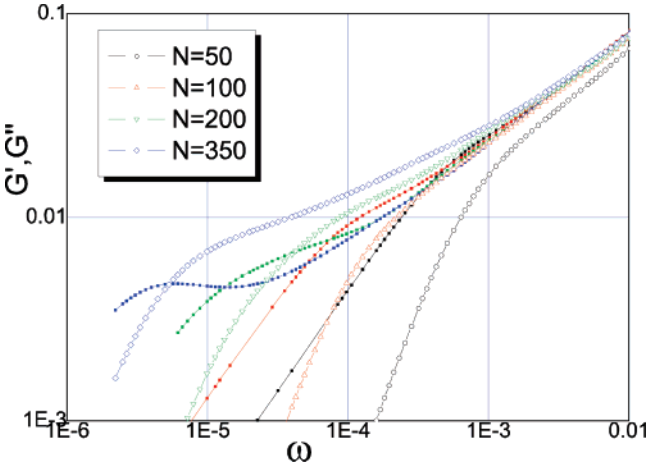

Figure 4. Storage and loss moduli obtained by Maxwell modes fit to the data from Figure 3.

Only the two longest chains $N = 200$ and $N = 350$ show clear deviations from the Rouse theory due to entanglements. The longest chain simulated deviates by a factor 2.5 above the Rouse "plateau" in this plot, which is significantly higher than the noise in the simulations. Thus, we argue that the presented data should be sufficient for determination of parameters describing entanglements (such as the tube diameter or the plateau modulus) by fitting it to an appropriate model. However, the model has to be accurate for small number of entanglements (e.g., $Z = 4$ and $Z = 7$ in our case), otherwise an extrapolation to large chain lengths will not be reliable. The quality of the stress relaxation data is good enough in order to transform them to storage and loss moduli by fitting $G(t)$ curves with a set of Maxwell modes. The results of this transformation are plotted in Figure 4 for the four longest chains investigated. The shapes of the curves are consistent with experimental data. The only qualitative disagreement is that the G' and G'' obtained from MD do not cross around τ_e, but are approximately parallel to each other for $\omega > 1/\tau_e$. In contrast to that, the experimental melt data always have $G'' > G'$ at high frequency. We will discuss this in more detail in the next section. Viscosity, zero-shear rate compliance, and terminal time (defined as the relaxation time of the slowest Maxwell mode) are reported in Table 1.

Although the effect of entanglements is significant, the longest chains are still far from the regime where reptation is dominant. The number of entanglements is so modest that quantitative comparison with the tube model is very dubious (see for example ref[13] for discussion of failure of the tube theory for short chains). Thus, we compare our results with the more detailed single chain slip−spring model,[3] which can help with

Table 1. Parameters of Simulated Systems Obtained from Stress Relaxation, Using Slip-Links Fitting (τ_0, M_0 and G_N^0), Primitive Path Analysis (G_{ppa}), and Maxwell Modes Fitting (τ_d, η and $J_N^{(0)}$)

k_b	ρ	C	p	τ_0	M_0	$G_N^{(0)}$	G_{ppa}	N	N_c	$10^{-3}\tau_{run}$	$10^{-3}\tau_d$	η	J_N^0
								50	30	400	6.9	33	17.6
3	0.85	4.12	0.286	0.88	0.624	0.058	0.044	100	70	1780	55	1880	26.5
								200	100	2090	770	23 000	30
								30	20	1277	2.3	133	13.6
5 (ev4)	0.85	3.6	0.36	0.98	0.644	0.0605	0.0396	50	20	879	5.2	294	14.2
								70	30	1000	26	911	23.8
								100	50	1250	76	2180	30.4
								50	100	147	2.8	95.4	22.1
1.5	0.85	2.57	0.46	1.11	0.953	0.0371	0.0235	100	50	1000	26	516	41.2
								200	70	925	105	2270	42.9
								50	20	895	3.2	106	21.5
3 (ev2)	0.85	2.17	0.54	4.27	1.613	0.0233	0.0195	100	50	1000	14	324	38.4
								200	70	1080	138	1750	70.4
								50	30	3977	2.8	89.4	22.8
1.1	0.85	2.3	0.51	3.04	1.48	0.025	0.0201	100	50	727	14	304	38.1
								150	50	553	56	788	57.2
								50	50	48	2	45	25
0	0.85	1.75	0.67	6.89	2.7	0.013	0.0103	100	50	1850	7.96	129	46
								200	70	1050	60	483	99
								350	100	3000	303	1960	128
								100	30	362	5.8	111	36.5
−3	0.85	1.44	0.82	16.6	4.14	0.0092	0.0063	200	50	972	21.9	269	64
								350	100	1080	117	874	113
								50	50	1240	7.4	309	16.4
0	1.05	1.57	0.607	23.5	2.24	0.0191	0.016	100	50	2620	44.8	843	38.6
								161	50	5071	145.3	2052	55.2
								241	70	3037	429	5594	68
								100	50	172	2.9	32.4	67.7
0	0.6	2.02	0.825	2.38	2.88	0.0094	0.005 68	200	50	307	9.37	77.4	102
								300	100	778	43.6	260	143

the extrapolation to longer chains. A more detailed comparison between molecular dynamics and the slip−spring model will be reported separately.[10]

The slip−spring model[3] is based on free Rouse chain characterized as usual by three parameters: statistical segment b, bead friction ζ and temperature T. Without loss of generality we set them to unity and use them to define the units of space, time and energy. Then in order to model entanglements, the slip−spring model adds a set of virtual springs, fixed in space at one end and attached to the Rouse chain by sliplinks, which slide freely along the chain with a friction much smaller than ζ. Thus, there are two entanglement-related parameters: the average number of chain beads between sliplinks, N_e and the number of beads in the virtual spring N_s (this defines the spring constant of each virtual spring, $k = 3k_BT/N_sb^2$). Careful choice of these two parameters will be discussed in the follow-up paper,[10] where we will show that the standard parameter set used in[3] is not the best choice to fit the detailed shape of the mean-square displacement. However, it is good enough for fitting the stress relaxation functions in order to obtain the plateau modulus.

We used a fitting procedure similar to the one in ref 3: we fix the slip-link parameters $N_s = 2$, $N_e = 16$ and $\zeta_s = 0.1$, precalculated stress relaxation $G(t)$ for different chain lengths, and then fitted the number of MD beads represented by one bead in the slip−spring model, M_0, and the elementary time scale, τ_0. The time τ_0 is just a horizontal shift in Figure 5, whereas M_0 determines the plateau modulus, the spectrum width and the shape of the curves. Note that we used 4 times more fine-grained simulations than in ref 3 in order to fit the short chains and early times more accurately. Figure 5 shows the best two parameter fit by the dotted lines. This set of slip-link parameters has a plateau modulus of $G_{sl} = 0.0367$ in units where $b = 1$ and $T = 1$. The plateau is defined as the plateau value of $G(t)$ of slip−spring model for infinite chain length. In practice, it is obtained by simulating long chains with no destruction of slip-links at the ends. The molecular dynamics stress signal was scaled by $\rho T/M_0$, where ρ is the monomer number density. The result of the fitting is $M_0 = 2.73$, $\tau_0 = 8$, which leads to the value $G_0 = 0.323$, corresponding to the plateau modulus $G_N^{(0)} = 0.012$. If we use G_0 as the third adjustable parameter, we can obtain better fits (solid lines in Figure 5), with parameters

$$G_0 = 0.354,\ M_0 = 2.7,\ \tau_0 = 7 \rightarrow G_N^{(0)} = 0.013$$

which has the combination $G_0M_0/\rho = 1.12$. The mean square

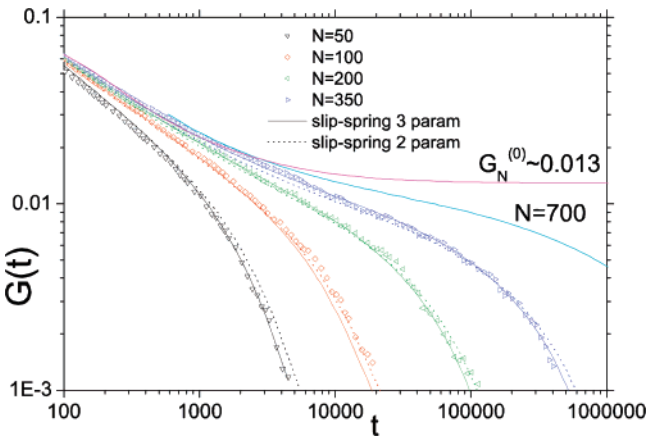

Figure 5. Best fit of MD results (symbols) for the four longest chains with the slip−spring model, using two fitting parameters G_0 and τ_0 (dashed lines) and three fitting parameters G_0, τ_0 and M_0 (solid lines), together with its predictions for $N = 700$ and $N \rightarrow \infty$.

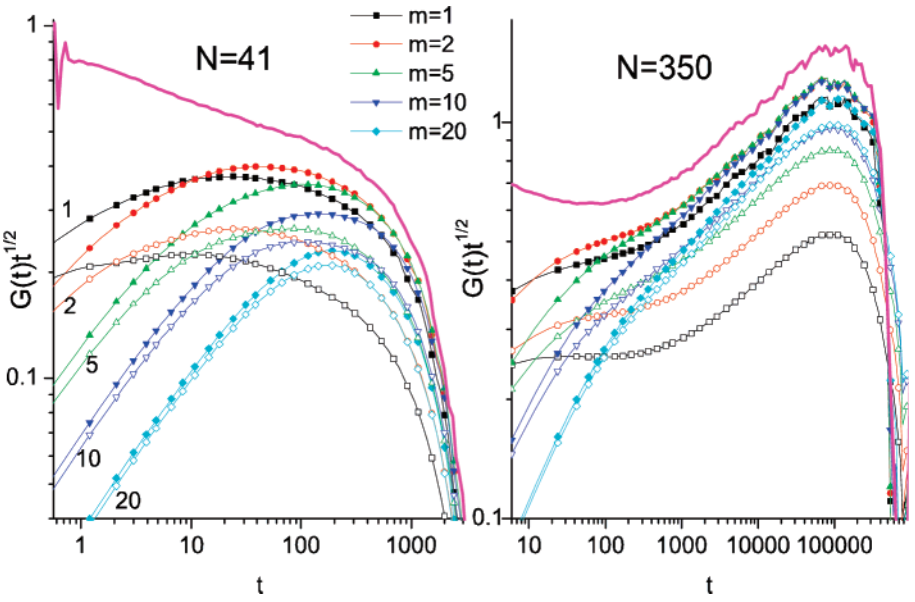

Figure 6. Normalized total stress (lines) for the standard KG model for $N = 41$ (left) and $N = 350$ (right) compared with the Kramers stress expression for sub-strands of different length. Filled symbols include the crosscorrelations between different chains, whereas open symbols do not.

error of the fit is about a factor of 2 smaller than for the two parameter fit, and we believe that it gives more accurate predictions for the plateau modulus $G_N^{(0)} = 0.013$. The reasons for the 12% deviation in the relationship between G_0 and M_0 are discussed later. In order to make an approximate connection with the tube theory, we remind the reader that for large N the stress relaxation from the slip−spring model can be fitted with the linear theory of Likhtman and McLeish[15] to yield

$$M_e = 26.8M_0, \quad \tau_e = 832\tau_0, \quad G_e = 0.045G_0 \quad (c_\nu = 0.1) \tag{2}$$

These values were obtained from the best fit to the standard slip−spring simulations[15,16] (with $N_e = 4$, $N_s = 0.5$) and then scaling the obtained parameters by factors of 4, 16, and $^1/_4$, respectively. Thus, our estimates for the entanglement time in molecular dynamics is $\tau_e \approx 5800$ and for entanglement molecular weight (as defined by ref 15) is $M_e = 72$.

The value of the plateau modulus is more than a factor of 2 lower than the 0.03 reported by Sen et al.,[8] and it is 30% higher than that (0.0097) measured previously by actual deformation of the MD sample.[14] The latter disagreement can be explained by the fact that no extrapolation to infinite chain length was performed in ref 14. Our value for the plateau leads to an entanglement molecular weight $N_e = 4/5\ \rho T/G_N^{(0)} \approx 51.5$, if we use the standard tube theory definition.[1]

It is interesting to check if the long time stress correlations can be described by the usual Kramers formula for Gaussian chains

$$\sigma_{\alpha\beta}^{(1)}(j,t) = \frac{3T}{\langle b^2\rangle}\sum_{i=2}^{N}(R_{i,j}^{\alpha}(t) - R_{i-1,j}^{\alpha}(t))(R_{i,j}^{\beta}(t) - R_{i-1,j}^{\beta}(t));$$
$$\sigma_{\alpha\beta}^{(1)}(t) = \sum_{j=1}^{N_c}\sigma_{\alpha\beta}^{(1)}(j,t) \tag{3}$$

where $\langle b^2\rangle$ is the average mean square bond length. The autocorrelation function of this stress expression $G^{(1)}(t) = V/T\ \langle\sigma_{\alpha\beta}^{(1)}(t)\sigma_{\alpha\beta}^{(1)}(0)\rangle$ is shown on Figure 6 as filled squares for unentangled chains of $N = 41$ (left) and for entangled chains $N = 350$ (right). One can see that Kramers stress relaxation function is roughly proportional to the exact stress relaxation function for $t > 100$ and is lower by about 25% for both unentangled and entangled chains. However, if one assumes that the different chains are not correlated with each other and calculates the autocorrelation function of the Kramers stress separately for each chain

$$G_{decoupled}^{(1)}(t) = \frac{V}{T}\frac{1}{N_c}\sum_{j=1}^{N_c}\langle\sigma_{\alpha\beta}^{(1)}(j,t)\sigma_{\alpha\beta}^{(1)}(j,0)\rangle$$

one obtains a very different result as shown in Figure 6 by the open squares. Although the result is less noisy due to the averaging over many chains independently, it is substantially lower and not even proportional to the total modulus in the case of the entangled system. Thus, the cross-correlations between different chains, which are usually neglected in both the Rouse and the tube theories are especially important. Since these correlations also exist for unentangled chains, they cannot be attributed only to entanglements. We can also generalize the stress defined in eq 3 to subchains of arbitrary lengths

$$\sigma_{\alpha\beta}^{(m)} = \frac{3T}{\langle(R_i - R_{i-m})^2\rangle}\sum_{j=1}^{N_c}\sum_{i=0}^{\mathrm{int}((N-1)/m)-1}(R_{im+1}^{\alpha} - R_{(i+1)m+1}^{\alpha}) \times (R_{im+1}^{\beta} - R_{(i+1)m+1}^{\beta}) \tag{4}$$

where int(x) is the integer part of x. The autocorrelation functions for different strand lengths m are shown in Figure 6 in the same way as for $m = 1$: for the whole system and for each chain assuming that different chains are not coupled. Surprisingly, the results for the whole system collapse on top of each other at late times for $m = 2$, 5, 10 (especially for $N = 350$), but they still underestimate the amplitude of the full stress by about 15%. We argue that the strands of length $m = 20$ are already comparable to N_e and may cross entanglements, thus underestimating the stress. The decoupled stresses slowly approach the coupled stresses as the strand length increases, suggesting that the correlations between larger strands are less important. However, the strand length cannot be increased any further than 20 because the longer strands will cut through entanglements. The remaining 15% discrepancy between the Kramers stress

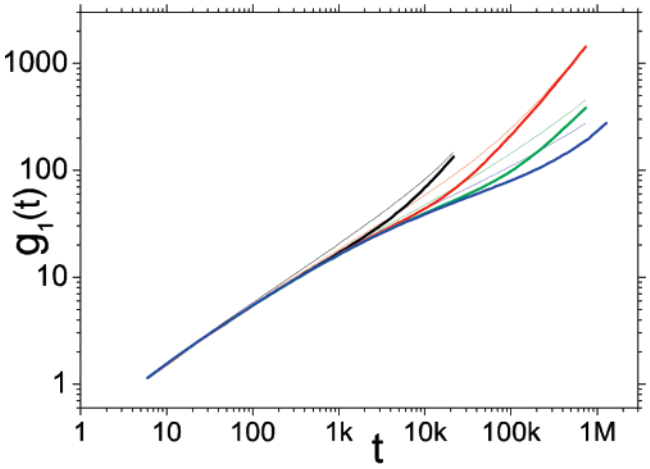

Figure 7. Monomer mean-square displacement (thin lines) and mean square central monomer displacement (thick lines) for $N = 50$, 100, 200, and 350 of the standard KG model.

expression and the total stress is probably due to the non-Gaussian character of the sub-strands. Although this error should decrease with increasing strand length, simulations of single chains with a nonzero bond length (bonded potential $U(r) = k/2(r - r_0)^2$ with $r_0 = 1$ and $k \gg 1$) show a very similar, i.e., 15% underestimation of the actual stress. This underestimation decreases very slowly with increasing chain and strand lengths.

3.2. Mean-Square Monomer Displacement. Another useful quantity traditionally measured in molecular dynamics is the monomer mean-square displacement $g_1(t)$, which is plotted in Figure 7 for the four largest chain lengths investigated. The popularity of this quantity among computer simulators can be directly traced to the predictions of Doi and Edwards.[1] They anticipated that this plot should show four different power laws depending on the regime, and the tube diameter a and the elementary time scale τ_e can be determined from the intersections of the power law fits. However, we find it very difficult to identify any clear power-laws on this plot, at least for mildly entangled systems ($Z \leq 7$) which can currently be simulated using molecular dynamics. To amplify different features of this plot, we calculate the mean-square displacement for every monomer in the system. To reduce the amount of information, we average these over groups of five monomers along the chain. We then divide this average by the Rouse power-law, $t^{1/2}$, and present the results in Figure 8 for the same 4 systems as shown in Figure 7.

First of all, we find that the picture is very rich and full of features. For example, $g_1(i, t)/t^{1/2}$ of some monomers show two maxima and two minima at intermediate times in the entangled systems. We assume that the negative slope in this plot is related to the slowing down due to entanglements as compared to the Rouse model. If we trace the motion of monomers 25−30 for $N = 350$ (thick line) we see that it first shows a negative slope (similar to the middle monomers) at around τ_e, when they first discover they are in a tube. At a later time, around $t = 10^4$, it shows a positive slope, which can probably be interpreted as the escape time from the tube. But then there is a second downturn: here the monomer discovers that it is connected to the other middle monomers, which are still inside the tube. To progress again as a fast speed, it has to wait for the center of mass motion, which happens at reptation time—the time of the final upturn of all the curves (it is actually higher than the terminal time of stress relaxation by a factor 1.4 for $N = 50$ and factor of 2 for $N = 350$). We hope that the richness of this behavior will make this plot useful for comparison between molecular dynamics and the single chain models (see ref[10]). Another point to notice is the absence of the second plateau predicted by the Doi−Edwards theory between the Rouse and the reptation times. We think this is due to two reasons. First, the reptation time of our longest chain is only about a factor of 3 larger than the Rouse time. Second, the change of slope expected at reptation time is 0.5, which is larger than the transition expected at τ_e and τ_R (0.25). In other words, the center of mass motion gives a strong signal, which obscures the subtle transition at Rouse time. Thus, the determination of the tube diameter from the transition at Rouse time proposed in ref[9] appears problematic.

The first transition at the Rouse time of one entanglement τ_e is slightly better defined, although it is clear that distinct power law regimes are not observed. For times $t < \tau_e$ we assume $g_1(i,t) \approx C_1 t^{1/2}$ where $C_1 = 0.543$ is the value of the first maximum in Figure 8 for the middle monomers. To get the prefactor C_2 in the relationship $g_1(i, t) \approx C_2 t^{1/4}$, we propose to calculate the mean-square displacement with respect to the center of mass, $g_2(i, t) = g_1(i, t) - g_3(t)$, where $g_3(t)$ is the mean-square displacement of the chain's center of mass. Then we plot this quantity for the middle monomers divided by $t^{1/4}$ in Figure 9—according to Doi−Edwards theory this plot should show a plateau for $\tau_e < t < \tau_R$. Since the data for our moderate chain lengths do not show a true plateau and do not collapse to the same curve, we define C_2 as the extrapolated value of the maximum of this plot to $N \rightarrow \infty$. Both the linear and quadratic in $1/N$ extrapolations are shown in the inset of Figure 9. The difference in the obtained asymptotic values provides some idea of the extrapolation error. The obtained value is $C_2 = 3.87 \pm 0.1$.

The tube diameter can be obtained from these two asymptotes (see the Appendix of ref 15) as

$$a = C_2\sqrt{\frac{3}{C_1}} \approx 9.1$$

The tube theory usually assumes that the chain of N_e monomers should have a mean end-to-end distance of a^2. This argument leads to $N_e = 49$ in striking agreement with the estimate from the plateau modulus. We think that the agreement is probably a coincidence since a priori there is no reason to expect that all the prefactors in the tube theory are correct. However, these findings contradict previous results by the Mainz group, who claimed that the plateau modulus leads to larger N_e than that obtained from $g_1(t)$. We also note that the slip−spring simulations of very long chains indicate that the plot in Figure 9 shows a maximum and then achieves a plateau (if any) at much longer times. This shows that any tube diameter values obtained from the mean-square displacement are very approximate.

4. Stress Contributions

Having discussed the result for the standard Kremer−Grest model, we can now ask: what are the different contributions to the stress relaxation function shown in Figure 2. It is obvious that at early times, $t < 1$,the bond length equilibration plays a huge role, being responsible for $G(t)$ starting at about 60, becoming negative several times before stabilizing at a value around 1. At long times the contribution must be polymeric in origin, i.e., arise due to the chain connectivity. However, the slope of $G(t)$ for $1 < t < 30$ is about −0.63—lower than the −0.5 slope predicted by the Rouse model. Is there a separate contribution responsible for this deviation?

In order to answer this question we would like to get rid of the oscillating bond relaxation contribution, which obscures the

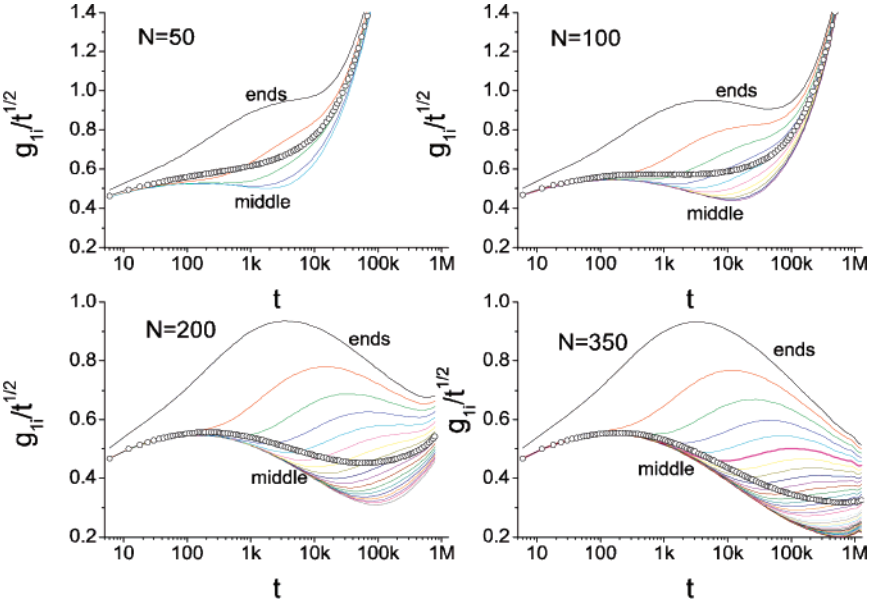

Figure 8. Monomer mean-square displacement, normalized by asymptotic Rouse slope of $t^{1/2}$ for each group of 5 monomers (lines). Open symbols shows averages over all monomers. A horizontal line on this plot corresponds to pure Rouse behavior.

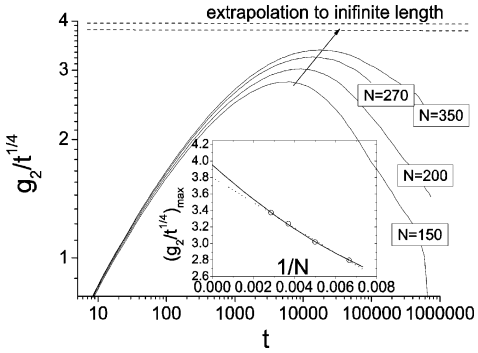

Figure 9. Mean-square displacement of the middle monomers with respect to the center of mass of the chain, normalized by reptation scaling $t^{1/4}$. Inset: extrapolation of the maximum of these curves to infinite chain length.

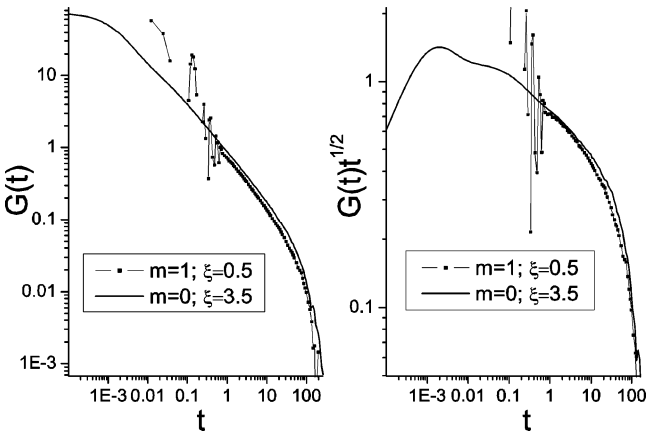

Figure 10. Stress relaxation for short chains $N = 10$ of the standard KG model (points) and of the same model without inertia and friction $\zeta = 3.5$.

features of interest in the $G(t)$ curves. One effective way to do so is to reduce inertia, which is ultimately responsible for the early time stress oscillations. In Figure 10, we show that setting the mass of the particles to zero and increasing the viscous friction to $\zeta = 3.5$ gives approximately the same stress relaxation for long times (the small horizontal shift still needed shows that our choice of $\zeta = 3.5$ is not exact). However, the stress

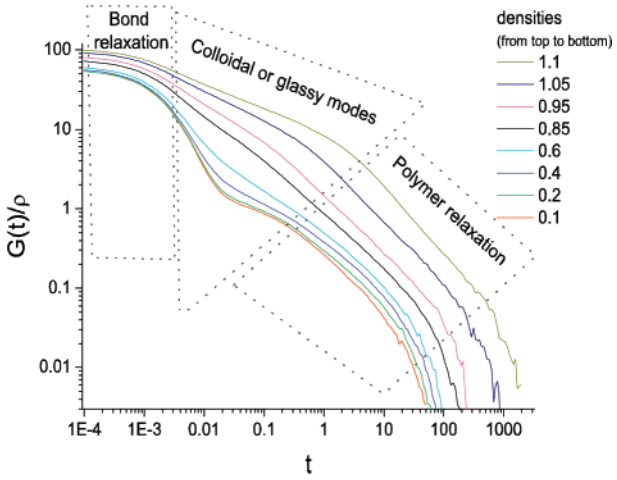

Figure 11. Stress relaxation normalized by the density for a system of short chains $N = 10$ with no inertia $m = 0$.

oscillations are absent and the bond length relaxation is shifted to earlier times compared to MD (making these simulations about 30 times more expensive). Indeed, in molecular dynamics the characteristic bond relaxation time is about $\tau = \sqrt{m/\kappa}$ where κ is the spring constant of the bond ($\kappa = 981$ for our FENE + LJ bonded potential), and in the Brownian case with zero mass $\tau = \zeta/\kappa$.

Right panel of Figure 10 shows a rescaled and thus zoomed in plot, which hints at the existence of a third process in between the bond relaxation process and the polymeric contribution: a small bump in the curve around $t = 0.1$. In order to confirm this, we performed Brownian dynamics simulations at different densities as shown in Figure 11. If we normalize $G(t)$ by the density, the low-density data collapse on top of each other clearly showing a two-step relaxation. Increasing density leads to the appearance of the third process, which we associate with colloidal or glassy interactions between Lennard-Jones spheres. Its range grows with growing density, thus pushing the polymeric stress relaxation to later times.

A similar situation is observed when changing the temperature but keeping the density constant at $\rho = 0.85$: the glassy or colloidal modes have a wider range at lower temperatures, as

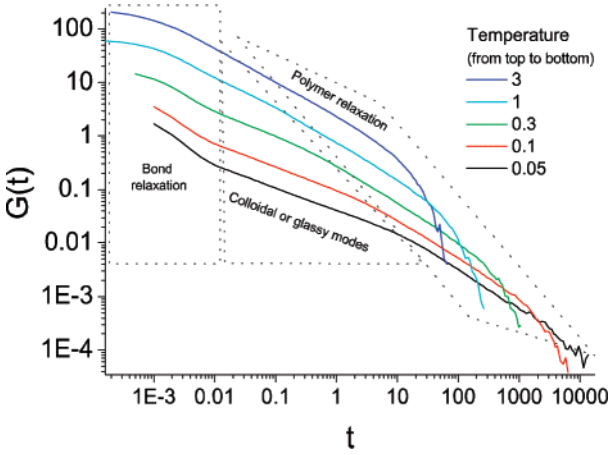

Figure 12. Stress relaxation for a system of short chains $N = 10$ with no inertia at different temperatures and constant density $\rho = 0.85$.

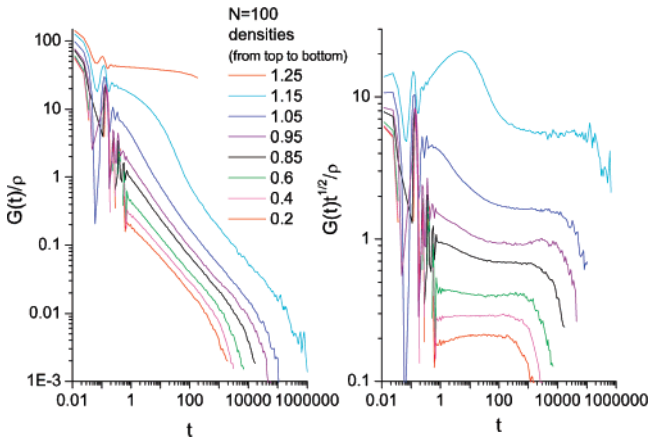

Figure 13. Stress relaxation for $N = 100$ standard Kremer−Grest model with inertia for different densities.

shown in Figure 12. This picture also shows that the amplitudes of different processes scale differently with temperature, making time−temperature superposition impossible. Indeed, the amplitude of the bond relaxation scales linearly with T, whereas overlaying the polymeric contribution requires vertical shift with approximately $T^{1.9}$ scaling. One should note that all simulations were performed at constant volume rather than constant pressure, so contrary to the usual experimental situation, the glass transition did not occur as we lowered the temperature. Further illustration of the glassy relaxation is shown in Figure 13, where simulation for longer chains $N = 100$ are presented at different densities with inertia ($m = 1$, $\zeta = 0.5$). On the right panel one can see that at the standard density $\rho = 0.85$ the deviation from the Rouse behavior for $t < 30$ can be explained by glassy modes, which disappear for $\rho = 0.4$ and $\rho = 0.2$. At higher densities the glassy peak becomes very pronounced, and the glass transition is observed at densities higher than $\rho = 1.2$ or so.

One can now ask the question: which simulation density corresponds to the usual polymer melts such as polystyrene, polyisoprene or polybutadiene? It is germane to note that for all these polymers experimental G' and G'' always cross each other at ω_{cross} around $1/\tau_e$, and G'' exceeds G' at frequency $10\omega_{cross}$ by a factor between 1.9 and 2.15 (e.g., $\tan\delta(10\omega_{cross}) \approx 2$). However, the storage and loss moduli from the standard Kremer−Grest model (Figure 4) do not cross each other and go parallel with a slope around $1/2$. This behavior does not change significantly for stiffer chains (see next section). The only way to rectify this is to increase the density. In fact, the system with the density $\rho = 1.15$ produces a shape of G' and G'' very similar to the experimental one. However, it is more expensive to simulate.

5. Chain Flexibility

The stress relaxation and the plateau modulus are strongly affected by the chemical structure of the chain, which can be mimicked in the crudest approximation by tuning the potential between bonded monomers. The packing model[17] suggests that the plateau modulus is determined only by the end-to-end vector R_0 and density ρ via

$$G_N^{(0)} \sim p^{-3}; \quad p = \frac{N}{R_0^2 \rho} \tag{5}$$

where p is a packing length. Here we would like to investigate the effect of bending potential and density on the plateau modulus and compare it with eq 5. We introduced the bending energy as an additional harmonic potential

$$U_{bend} = \frac{k_b}{2} \sum_{i=2}^{N-1} (r_{i+1} - 2r_i + r_{i-1})^2$$

In this way the forces are pairwise and the force on the particle i from the particles $j > i$ is

$$f_i = 4k_b(r_{i+1} - r_i) - k_b(r_{i+2} - r_i)$$

Thus, our bending potential corresponds to an attractive harmonic spring $4k_b$ between neighboring beads and a repulsive k_b harmonic spring between beads with chemical distance 2.

Figure 14 shows the stress relaxation curves for different molecular weights and bending energies. Table 1 lists the different systems investigated and the parameters obtained by fitting $G(t)$ with the slip−spring model. We varied the bending energy from $k_b = 3$ to $k_b = -3$, and also simulated two systems where the bending potential was not applied to every second or every fourth monomer (with $k_b = 3$ and $k_b = 5$ respectively). Another system included in the table and the figures is a system with no bending energy, but with a different density, $\rho = 0.6$. We fitted all the molecular weights of the same structure simultaneously with the slip−spring model without bending energy. We used $N_e = 16$ and $N_s = 2$, $\zeta_s = 0.1$, corresponding to a model 4 times more fine-grained than the one used in ref 3. This was necessary in order to fit early time stress relaxation more accurately. The fits were performed in two ways. The first method involves optimizing two parameters G_0 and τ_0, and then calculating the molecular weight in MD corresponding to one bead in the slip−spring model as

$$M_0 = \frac{\rho T}{G_0} \tag{6}$$

This formula effectively assumes entropic elasticity at long time scales (see[3]). The fits using this method are shown in Figure 14 by lines. The second method is to let M_0 be the third fitting parameter. We found that the most stable and reliable fits were obtained when the mean square fitting error was calculated in linear coordinates for the plot $\sqrt{t}G(t)$, and MD data were ignored for $t \lesssim 0.1\tau_e$. The fits are satisfactory apart from a small discrepancy for the stiffest chains around τ_e. We used the parameter G_0 in order to get the plateau modulus $G_N^{(0)}$ for infinitely long chains by multiplying it by 0.0367, which is the value of the $G(t)$ from the slip−spring model with the specified parameters for long time and infinite chains.

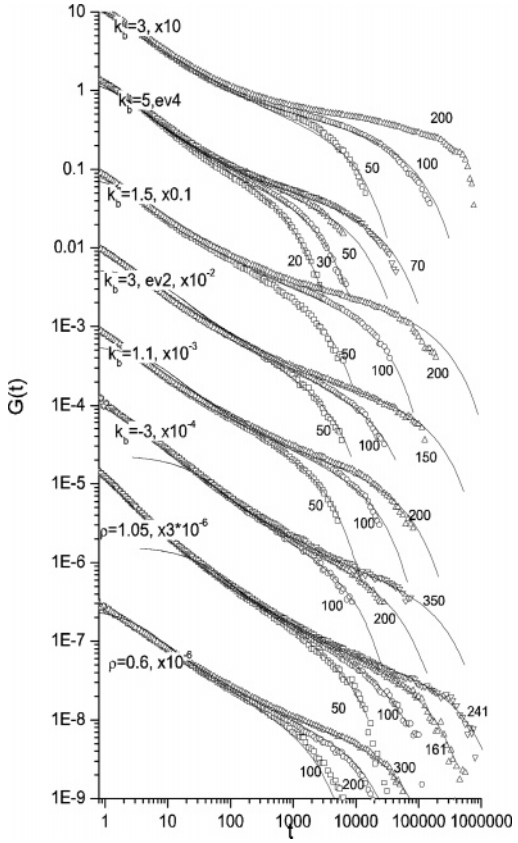

Figure 14. Stress relaxation for systems with different bending potentials. If just bending energy k_b is specified, it is applied to every monomer. The labels ev2 or ev4 mean that the bending potential is not applied to every second or every fourth monomer. Lowest two groups of curves are for systems without bending but with different density $\rho = 1.05$ and $\rho = 0.6$.

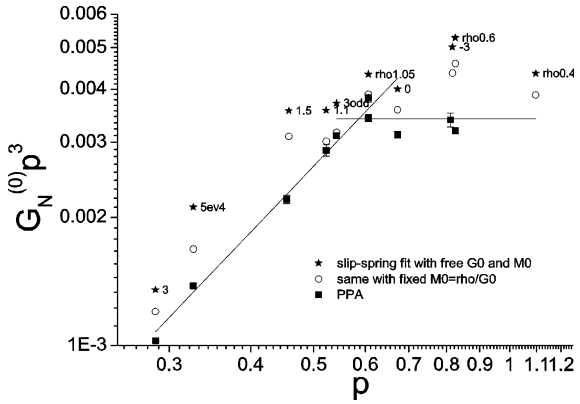

Figure 15. Plateau modulus normalized by the cube of the packing length for systems with different bending energies or densities. Key: stars, results from the slip-links fits with independent M_0 and G_0 (fits shown in Figure 14); circles, fits with M_0 calculated from eq 5; squares, results from the primitive path analysis. Lines correspond to predicted scaling laws $G_N^{(0)} \sim p^{-7/5}$ for the semiflexible chains and $G_N^{(0)} \sim p^{-3}$ for the flexible case. Lables refer to systems listed in Table 1. The point for $\rho = 0.4$ results from chains $N = 300$ and shorter, having too few entanglements to yeild reliable PPA prediction. The error bar for this point is larger than for other points.

Figure 15 shows the obtained plateau modulus normalized by the cube of the packing length as a function of packing length using both methods. It also includes the results from the primitive path analysis (PPA)[14] performed on the final configurations of the longest chains simulated for each system using ESPResSo.[18] The PPA procedure is described elsewhere.[14] Several important conclusions can be drawn form Figure 14. First of all, letting M_0 and G_0 be independent leads to the plateau modulus, which is about 15% larger than those obtained using eq 6. This is consistent with results analyzed in Figure 6, where we showed that the stress assuming Gaussian strands is about 15% lower than the actual stress. We thus conclude that the second method (letting M_0 and G_0 be independent) gives more precise estimate of the plateau modulus. The fits are also of course better because one more parameter is used, thus providing more unique results. Fitting with the slip−spring model gives results proportional to those from the PPA for semiflexible chains, the first being about 30%−40% higher plateau modulus than the second. It looks like the PPA systematically underestimates the plateau modulus. Within the experimental error, the systems investigated so far lie on a mastercurve if $G_N^{(0)}$ is plotted as a function of packing length. However, it is desirable to accurately simulate more systems to verify this statement. It is also desirable to find the limits of its applicability. For semiflexible chains, the results are consistent with the scaling $G_N^{(0)} \sim p^{-7/5}$, predicted by Semenov.[19] The scaling behavior $G_N^{(0)} \sim p^{-3}$ observed by Fetters et al.[17] experimentally is obtained only for chains with negative stiffness or lower densities and only from PPA results. The results from the slip−spring model do not reach asymptotic behavior $G_N^{(0)} \sim p^{-3}$ at least for our systems. The standard Kremer−Grest model without bending already lies at the transition region from flexible to semiflexible chains. However, a vast majority of synthetic polymers collected by Fetters et al.[17] do not show significant deviations from $G_N^{(0)} \sim p^{-3}$ law. This (together with the G'/G'' behavior at high frequencies discussed in the previous section) leads us to question the applicability of the standard parameters of the Kremer−Grest model (especially with positive bending) for quantitative modeling of the usual flexible synthetic polymers. However, it is perfectly suited for model development and testing.

6. Conclusions

We have proposed an effective way to calculate time-correlation functions in multichain molecular dynamics simulations. Using this method, we have calculated stress−stress autocorrelation functions for a wide variety of unentangled and entangled systems of a bead−springs model with and without bending energy. In order to obtain the plateau modulus of each system, we fitted the stress relaxation $G(t)$ with the slip−spring model, which describes mildly entangled chains much better than the tube model. We also performed the primitive path analysis on all final configurations. The obtained plateau modulus is very similar to those obtained from the slip-links fitting. As a function of packing length, it follows p^{-3} law for low densities or negative bending energy, and $p^{-7/5}$ law for positive bending energy. The standard Kremer−Grest model without bending lies at the transition between these two regions.

The quality of the $G(t)$ signal is sufficient in order to calculate the loss and storage moduli. At the usual density $\rho = 0.85$ they do not cross at high frequency around $1/\tau_e$ and go parallel with about $^1/_2$ slope. This contradicts the linear rheology of polymer melts, where G'' always crosses G' and exceeds it by a factor of 2 or so at higher frequency. The bending energy does not improve this, and only a significant increase in density up to $\rho = 1.15$ or so can rectify this disagreement. In order to highlight the role of different processes in stress relaxation, we switched off inertia by setting mass to zero and systematically varied the density and the temperature in the *NVT* ensemble. We identified three processes which affect stress relaxation in the

Kremer−Grest model: bond length relaxation, colloidal or glassy mode due to collisions with different atoms (and probably some collective cage motion at high densities), and polymeric relaxation. The latter can be subdivided into Rouse and reptation parts.

We have also analyzed the Kramers expression for the stress, which includes only the intrachain contributions (although the interchain interactions affect the end-to-end distance of the strands in eq 4). If applied to subchains of various lengths from 2 to 20, it gives the result proportional to the true $G(t)$ but underestimates it by about 15%. However, if cross-correlations between different chains are neglected, the result is very different and is not even proportional to the true stress relaxation at long times. This fact poses a serious challenge to the tube theory, which assumes that the relaxation of each chain is independent from that of the surrounding chains. It also shows that at least the prefactor in the relationship between the plateau modulus and the molecular weight between entanglements is not trivial. However, the asymptotic value for $N_e = 49$ obtained from the mean square monomer displacement for the standard model without bending is in good agreement with the one obtained from the plateau modulus. Unfortunately, the analysis of the mean-square displacement we have presented cannot be extended to chains with bending energy since the shapes of $g_1(t)$ and the scaling laws are strongly affected by the bending energy.

We hope that although this paper does not provide any answers to the open questions of entangled dynamics, it will provide a useful starting point for molecular dynamics simulations studies in this direction. In particular, we demonstrated that stress relaxation function can be now routinely accessed and compared with the competing tube or slip-links models. The next paper[10] will be dedicated to a detailed comparison between molecular dynamics and the slip−spring model.

Acknowledgment. We thank Benoit Loppinet for introducing us to photon correlation spectroscopy correlators as well as Daniel Read and Richard Graham for useful discussions. This work was supported by EPSRC, Grant GR/S94711 (S.K.S.), Microscale polymer processing grant (J.R.) and Advanced EPSRC fellowship (A.E.L.).

References and Notes

(1) Doi, M.; Edwards, S. F. *The Theory of Polymer Dynamics*; Clarendon: Oxford, U.K., 1986.
(2) McLeish, T. C. B. *Adv. Phys.* **2002**, *51*, 1379−1527.
(3) Likhtman, A. E. *Macromolecules* **2005**, *38*, 6128−6139.
(4) Kremer, K.; Grest, G. S. *J. Chem. Phys.* **1990**, *92*, 5057−5086.
(5) Gao, J.; Weiner, J. H. *Macromolecules* **1989**, *22*, 979−984.
(6) Karayiannis, N.; AE, A. G.; Mavrantzas, V.; Theodorou, D. *J. Chem. Phys.* **2002**, *117*, 5465−5479.
(7) Auhl, R.; Everaers, R.; Grest, G. S.; Kremer, K.; Plimpton, S. J. *J. Chem. Phys.* **2003**, *119*, 12718−12728.
(8) Sen, S.; Kumar, S. K.; Keblinski, P. *Macromolecules* **2005**, *38*, 650−653.
(9) Zhou, Q.; Larson, R. G. *Macromolecules* **2006**, *39*, 6737−6743.
(10) Sukumaran, S. K.; Likhtman, A. E. Manuscript in preparation.
(11) Magatti, D.; Ferri, F. *Appl. Opt.* **2001**, *40*, 4011−4021.
(12) Sukumaran, S. K.; Ramirez, J.; Likhtman, A. E. 2007, manuscript in preparation.
(13) Liu, C.; He, J.; Keunings, R.; Bailly, C. *Macromolecules* **2006**, *39*, 3093−3097.
(14) Sukumaran, S. K.; Grest, G. S.; Kremer, K.; Everaers, R. *J. Polym. Sci., Part B: Polym. Phys.* **2005**, *43*, 917−933.
(15) Likhtman, A. E.; McLeish, T. C. B. *Macromolecules* **2002**, *35*, 6332−6343.
(16) Ramirez, J.; Sukumaran, S. K.; Likhtman, A. E. *Macromol. Symp.* **2007**, *252*, 119−129.
(17) Fetters, L. J.; Lohse, D. J.; Graessley, W. W. *J. Polym. Sci., Part B: Polym. Phys.* **1999**, *37*, 1023−1033.
(18) Limbach, H.-J.; Arnold, A.; Mann, B. A.; Holm, C. *Comput. Phys. Commun.* **2006**, *174*, 704−727.
(19) Semenov, A. N. *J. Chem. Soc., Faraday Trans.* **1986**, *82*, 317−329.

MA070843B